

DESIGN AND TESTING OF A BUOYANT UAV FOR AGRICULTURAL SURVEILLANCE

Pruthvi P. Kapoor[1], Rajkumar S. Pant[2], Mustafa Abdelrahman[1], Diana Mohd-Nasir[3] & Mohammed S. Ismail[1]

[1]University of Hull, Cottingham Road, Hull, HU6 7RX, United Kingdom
[2]Indian Institute of Technology Bombay, Mumbai, Maharashtra, 400076, India
[3]University of Sheffield, Sheffield S1 3JD, United Kingdom

Abstract

Precision agriculture relies on Unmanned Ariel Vehicles (UAVs) for high-resolution crop monitoring, but conventional multirotor platforms are limited by short flight times, typically 20 to 30 minutes per battery cycle and the propellor downwash disturbing the crop and the image they are meant to capture. This paper presents the design and initial testing of a buoyant UAV that addresses these problems at once. The platform uses a 2.0 m diameter, 0.5 m height toroidal lenticular envelope filled with hydrogen, supported by a concentric carbon fibre structure and propelled by three brushless motors. Hydrogen was chosen as the lifting gas because it delivers roughly 8 % more specific lift than helium, it also costs five to ten times less and is far more readily available; the safety implications are addressed through envelope-material selection, gas-cell construction and operational procedure. We derive a closed-form analytical formula for the envelope volume of the chosen geometry, present a complete mass and lift budget, and document the built and first flight of sub-scale and full-scale prototypes. With the envelope sized to V = 0.9529 m^3, hydrogen buoyancy carries 86 % of the all-up mass of 1106 g, leaving the propulsion system to supply only the small residual thrust required for flight and control. The result is a development pathway towards a hover endurance well beyond the current multirotor norm, with negligible downwash and low altitude near canopy flights over crops.

Keywords: Buoyant UAV, Hybrid airship, Hydrogen lifting gas, Toroidal lenticular envelope, Precision agriculture

Nomenclature:

D	=	Major axis (outer) diameter of envelope (m)
D_{gap}	=	Central bore diameter (m)
L	=	Gross aerostatic lift (g)
L_n	=	Net effective lift margin (g)
L_{tail}	=	Tail (parabolic section) length (m)

L_{gross}	=	Computed gross lift (g)
L_{tip}	=	Total radial half-length from axis to tail tip (m)
M	=	Molar mass of the lifting gas (hydrogen, 2.01588 × 10^{-3} kg/mol)
P	=	Ambient atmospheric pressure (Pa)
R	=	Profile radius of the semicircular nose (m)
R_u	=	Universal gas constant (J/(mol·K))
T	=	Ambient temperature (K)
t	=	Maximum height / minor axis of envelope (m)
u	=	Integration substitution variable (m)
v	=	Generic enclosed volume of a solid of revolution (m^3)
V_{nose}	=	Volume contribution from nose (semi-circular) region (m^3)
V_{tail}	=	Volume contribution from tail (parabolic) region (m^3)
V_{total}	=	Total enclosed gas volume (m^3)
W	=	Total system mass (kg)
x	=	Radial coordinate measured from the central axis of revolution (m)
x_c	=	Radial distance from axis of revolution to nose center (m)
$y(x)$	=	Envelope profile half-height at radial distance (m)
$y_{nose}(x)$	=	Profile half-height in the nose region (m)
$y_{tail}(x)$	=	Profile half-height in the parabolic tail region (m)
Φ	=	Fineness ratio = D / t
ρ_{air}	=	Ambient air density (kg/m^3)
ρ_{he}	=	Helium gas density (kg/m^3)
ρ_{h2}	=	Hydrogen gas density (kg/m^3)

1. Introduction

Precision agriculture has become one of the most active application areas of small UAVs, with reviews confirming that UAV remote sensing now exceeds what satellites can provide for early crop diagnostics [1]. Two limitations still dominate the workflow, and both stem from the same airframe. The first is endurance: a standard quadcopter provides approximately 20 minutes of hover per battery cycle, with recent measurements putting the figure at 18 minutes as tested by [2]. The second is propellor-induced downwash. Yang et.al. [3] quantified the effects for a six-rotor agricultural platform and found it enough to motivate explicit standoff distances in operational guidelines and the closer the multirotor gets to the canopy, where the highest value measurements lie, the worse the wash gets.

A lighter than air (LTA) platform inverts both problems. A sealed envelope of low-density LDPE material carries most of the airframe weight, so the motors run at a small fraction of their rated thrust at hover. The platform is built around three deliberate choices: a toroidal lenticular envelope that packs the buoyant volume into a flatter, aerodynamically isotropic shape with a central bore for vertical lift provided by the motor mounted in the centre. Second being hydrogen used as the lifting gas, which delivers about 8% more specific lift than helium and costs a lot less too [4,5]. Third being a three-motor configuration propulsion system mounted on a concentric carbon-fibre ring frame.

This paper derives a closed-from analytical formula for the envelope volume, presents a complete mass and lift budget for the platform (computed both rigorously against International

Standard Atmosphere (ISA) and conservatively against 1 g per litre rule), compares candidate envelope materials, documents the build, and first flight of a working prototype.

2. Literature Review

2.1 Lenticular and Disk-Shaped Airships

The lenticular family covers any disk-shaped solid of revolution, and its appeal for airships is twofold: the shape is aerodynamically isotropic in yaw (a useful property for slow station-keeping in variable wind), and it packs a large gas volume into a flat profile that is comparatively easy to manufacture. Kanoria et al. [6] ran a parametric CFD study across fineness ratios from 1 (sphere) to 7 (flat disk) and identified $\Phi \approx 5$ as the drag-optimal point, with envelope-volume reductions of around 50% at equivalent payload compared with a spherical envelope. The historical record reinforces the engineering case: the CNRS Pégase stratospheric lenticular airship, with its hexagonal geodesic cell structure and large-scale wind-tunnel validation [7], and the Russian DKBA-27 “Anyuta”, a 16-meter lenticular hull capable of a 100 kg payload [8], demonstrated that the form factor scales from indoor prototypes up to full-size cargo lifters. At the small-scale end, the OSIRCA platform from IIT Bombay [9] showed that a 2 m oblate spheroid airship could be built from radio-frequency-sealed coated-PVC petals and flown indoors with three-motor thrust vectoring, a direct heritage line for the present work The modern hybrid-airship literature, well surveyed by Bock et al. [10] and reviewed in depth by Manikandan and Pant [11], confirms that lenticular multi-lobed hulls remain technically attractive whenever a combination of static lift and dynamic-lift augmentation is needed.

2.2 Small Hybrid LTA UAVs

Compact buoyant UAVs are a niche but rapidly maturing category. The S-CLOD platform of Song et.al. [12,13] is the closest direct precedent of the present work, a 35-micron PET torus, approximately 2 m in diameter, holding 1.3 m^3 of helium and achieving about 63 minutes of sustained flight against a 20-minute quadcopter baseline. The same group has since extended the architecture to a torus-type omni-directional blimp using tilting actuators [14]. The Georgia Tech Miniature Autonomous Blimp (GT-MAB) of Cho et.al. [15] sits at the opposite end of the size envelope: an 85.9 g spherical helium blimp with 12.1 g useful payload and a flight time of up to two hours per charge, controlled by a switched autopilot and, in later work by Seguin et al. [16], localized onboard by a convolutional neural network. Pursuing a more radical propulsion approach, Yamada et.al [17] built ZeRONE, a roughly 90 cm helium drone that uses piezoelectric microblowers to eliminate rotor blades altogether. Across this small fleet, the consistent finding is that the buoyant-versus-thrust trade favours buoyancy as the platform shrinks: smaller motors at lower throttle settings beat larger motor at higher settings, and endurance follows directly.

Marcias and Lee [2] provide the cleanest quantitative benchmark for a hybrid architecture: by mounting a helium filled balloon to a quadcopter, they raised the endurance of the combined system from 18 minutes (quadcopter alone) to 46 minutes, a factor of 2.56. Their comparison between fixed-angle and ball-and-socket joint coupling is also a useful design-trade reference. The point that follows from all these prior platforms, and that present paper builds on is that helium delivers the endurance gain at a substantial recurring cost.

Replacing it with hydrogen offers an 8 % lift bonus and an order-of-magnitude cost reduction, which is the trade we take in this work.

2.3 Hydrogen as a lifting gas

After the Hindenburg disaster, hydrogen was effectively displaced by the helium in Western airship operations. In the modern context where helium is both expensive and supply constrained, the case for hydrogen has been revisited carefully. Bock and Künkler proposed a hydrogen-filled lenticular hybrid airship as a multi-mode platform [4], and the standard engineering treatment by Khoury and Gillett in their reference text on airship technology [18] gives the gas-handling and envelope-design framework that any modern hydrogen LTA design should follow. NASA's Ballon Program Office returned to hydrogen for scientific ballooning in 2025 and quotes two numbers directly relevant to the present work: a typical 5 - 10 x cost reduction relative to helium, and an approximately 8 % gain in available lift at equivalent envelope conditions [5]. The dominant hazards for a sealed hydrogen envelope are not in-flight combustion (which would require both an ignition source and an oxidant inside the envelope) but ground handling, leakage into confined spaces and rapid venting on rupture, all of which amenable to standard operating procedure, and all of which are addresses in Section 8.

3. Design Requirements

The platform was specified to support a near canopy precision-agriculture sensing mission: low-altitude hover above an open agricultural field, a few meters above the canopy, with sufficient endurance to cover a representative field in a single shortie and sufficient capacity for a multispectral sensor. The hover speed ceiling is set to preserve image quality and minimize crop disturbance, the envelope diameter capped at 2.0 m, so the platform fits within standard row-crop inter-row spacings, and all up mass is held below 1.2 kg. Table 1 summarises the resulting requirements: the 90-minute maximum endurance target is set deliberately at roughly twice the 46-minute figure achieved by the helium assisted hybrid quadcopter [2].

Table 1 Key design requirements

Design requirement	Value	Units
Payload (sensors + camera)	0.5	kg
Maximum hover endurance	90.0	minutes
Maximum hover speed	5.0	m/s
Operating above crop canopy	1.0 to 5.0	m
Maximum envelope diameter	2.0	m
Maximum envelope height	0.5	m
Maximum all-up mass	1.2	kg
Target buoyancy to weight ratio	≥ 0.85	-

4. Envelope Geometry and Volume Derivation

4.1 Profile definition

The envelope is a solid of revolution generated by rotating a cross-sectional profile about the central vertical axis. The profile has a semicircular nose of radius R, centred at a radial offset x_c from the axis, and a parabolic tail that runs from the joining at $x = x_c$ out to a sharp tip at $x = L_{tip}$. The parabolic tail is chosen because it is tangent to the nose at the join (so there is no curvature discontinuity) and because the gentle adverse pressure gradient on the parabolic afterbody suppresses the trailing-edge separation that would otherwise dominate the drag of a blunt-ended disk. Figure 1 shows the cross-section with the three governing parameters R, x_c and $L_{tail} = L_{tip} - x_c$.

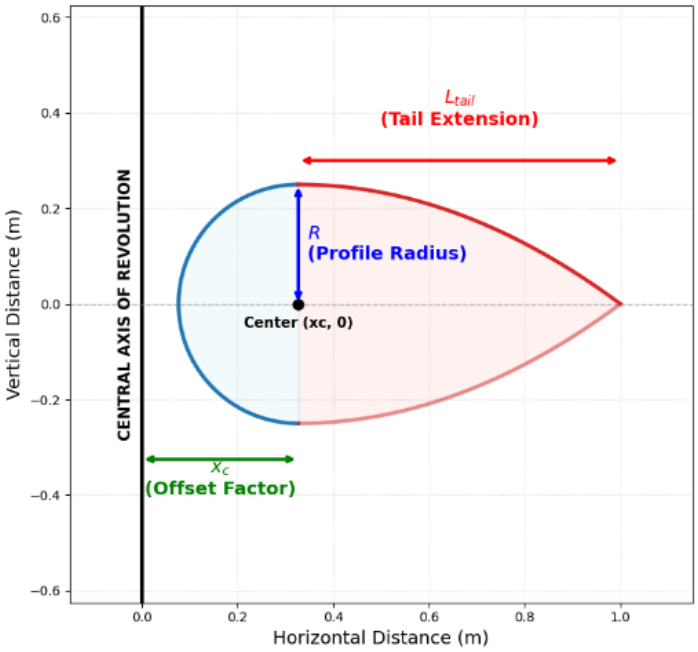


Figure 1 Cross-section of the envelope geometry

4.2 Profile equations

The profile height $y(x)$ is piecewise. Across the semicircular nose region, $x \in \left[\frac{Dgap}{2}, x_c\right]$:

$$y_{nose}(x) = \sqrt{[R^2 - (x - x_c)^2]} \tag{2}$$

Across the parabolic tail region, $x \in [x_c, L_{tip}]$:

$$y_{tail}(x) = R\left[1 - \left(\frac{(x - x_c)}{L_{tail}}\right)^2\right] \tag{3}$$

Equation (3) is tangent to the nose at x_c and pinches to a point at $x = L_{tip}$, which is the sharp tip condition that minimises trailing edge separation.

4.3 Volume derivation

The enclosed volume is computed by the shell method. A thin cylindrical shell at radius x with height $2y(x)$ and thickness dx contributes, $2\pi \cdot x \cdot 2y(x) \cdot dx$, so the total volume is

$$V = 4\pi \int x \cdot y(x)\, dx \tag{4}$$

decomposed into nose and tail contributions, $V_{total} = V_{nose} + V_{tail}$.

The nose volume is obtained most cleanly from Pappu's second theorem. The cross section is a semicircle of area $\frac{\pi R^2}{2}$: it's centroid lies at radial distance $x_c - \frac{4R}{3\pi}$ from the axis and revolves through $2\pi\left(x_c - \frac{4R}{3\pi}\right)$. Multiplying:

$$V_{nose} = \pi^2 R^2 x_c - \left(\frac{4}{3}\right)\pi R^3 \tag{5}$$

The tail volume comes from substituting Equation (3) into Equation (4) and integrating from x_c to $x_c + L_{tail}$. With substitution $u = x - x_c$ the integral closes in elementary form:

$$V_{tail} = \pi R L_{tail}\left[\left(\frac{8}{3}\right)x_c + L_{tail}\right] \tag{6}$$

Adding (5) and (6) gives a single closed form expression for the envelope volume:

$$V_{total} = \pi R\left[\left(\pi R x_c - \left(\frac{4}{3}\right)R^2\right) + L_{tail}\left(\left(\frac{8}{3}\right)x_c + L_{tail}\right)\right] \tag{1}$$

with R the nose profile radius, $x_c = \frac{D_{gap}}{2} + R$ the offset, and $L_{tail} = L_{tip} - x_c$ the tail length. Equation (1) is the central design loop kernel of this paper: given a target lift, an inversion of (1) return the envelope dimensions directly rather than via iterative back solving from the buoyancy equation.

4.3 Numerical verification

The design inputs for the prototype are D = 2.0 m, t = 0.5 m and D_{gap}= 0.1542 m, giving fineness ratio $\Phi = \frac{D}{t}$ = 4 (close to but slightly below the drag optimum $\Phi \approx 5$ of [6], chosen to keep the envelope height down for ground handling). Substituting these into Equation (1):

$$V_{total} = \pi \times 0.25 \times \left[\begin{array}{l}\left(\pi \times 0.25 \times 0.3271 - \left(\frac{4}{3}\right)0.25^2\right) \\ +0.6729 \times \left(\left(\frac{8}{3}\right) \times 0.3271 + 0.6729\right)\end{array}\right] = 0.9529\ \mathrm{m}^3 \tag{7}$$

This matches the CAD measurements of 0.9529 m^3 shown in Figure 2 to four decimal places, confirming both the derivation and the implementation. The principal geometric parameters are summarised in Table 2.

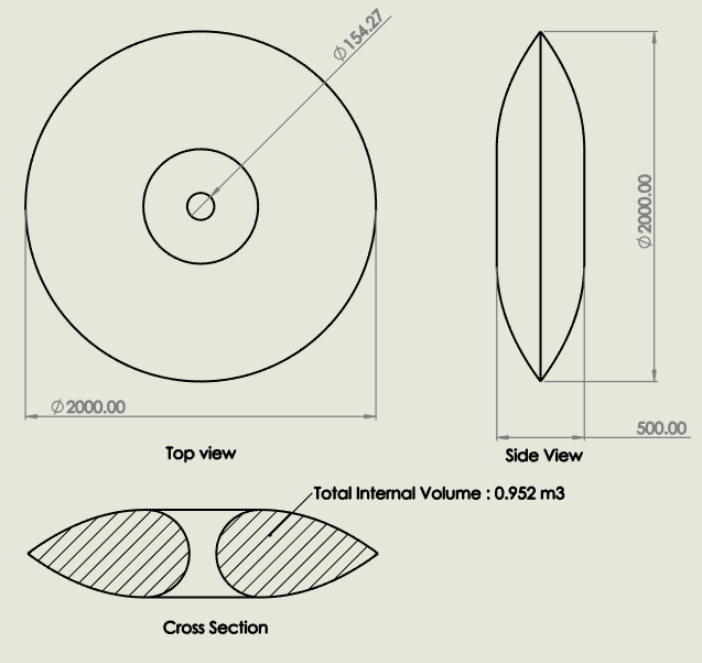


Figure 2 CAD drawings of the proposed design

Table 2 Principal geometric parameters of the envelope

Parameter	Value	Units
Major axis diameter, D	2.0	m
Maximum height, t	0.5	m
Fineness ratio, Φ	4.0	-
Profile radius, R	0.25	m
Central bore diameter, D_{gap}	0.1542	m
Centre offset, x_c	0.3271	m
Half length, L_{tip}	1	m
Tail length, L_{tail}	0.6729	m
Envelope volume, V_{total}	0.9529	m^3

5. Hydrogen Lift Calculation

Aerostatic lift follows Archimedes's principle: the gross lift produced by a sealed envelope of volume V is the product of V and the density difference between the displaced air and the contained gas,

$$L = V \cdot \left(\rho_{air} - \rho_{H_2}\right) \tag{8}$$

At ISA sea level conditions (288.15 K, 101.325 kPa) the ambient air density is ρ_{air} = 1.225 kg/m^3. The hydrogen density at the same conditions, computed from the ideal gas law with molar mass M = 2.01588 g/mol and the universal gas constant R_u = 8.314 J/(mol·K), is

$$\rho_{H_2} = \frac{PM}{R_u T} = \frac{101325 \times 2.01588 \times 10^{-3}}{(8.314 \times 288.15)} = 0.0852 \frac{\text{kg}}{\text{m}^3} \quad (9)$$

giving a specific lift of 1.225 – 0.0852 = 1.140 kg/m^3. For the envelope of volume 0.9529 m^3 from the Equation (7), the gross lift therefore

$$L_{gross} = 0.9529 \times 1.140 = 1.086\,\text{kg} = 1086\,\text{g} \quad (10)$$

For helium at the same conditions (ρ_{He} = 0.169 kg/m^3, scaled from the 0 degree C reference value), the same envelope would deliver 1.225 – 0.169 = 1.056 kg/m^3 = 1006 g i.e. about 80 g less, confirming the 8 % advantages quoted by NASA in [5].

In practice the realised lift sits a few percent below the ISA-rigorous figure. Three effects account for the gap: industrial-grade hydrogen is typically 99.9 % rather than 100 % pure, the envelope warms under solar load (which reduces gas density along with ambient density, but not by the same fraction), a small pressure differential at inflation reduce the effective net buoyancy. A conservative engineering rule of thumb used widely in the LTA systems is “1 g of lift per litre of envelope volume,” which of the present envelope evaluates to 953 g. We size the platform against this conservative figure in what follows: 133 g headroom between conservative and rigorous values is treated as a margin against in-flight envelope warming and gas-purity loss. Table 3 summarises the lift figures.

Table 3 Hydrogen lift budget at ISA sea-level conditions

Parameter	Value	Units
Envelope volume	0.9529	m^3
Ambient air density (ISA SL)	1.225	kg/m³
Hydrogen Density (15° C, ideal gas)	0.0852	kg/m³
Specific Lift	1.140	kg/m³
ISA-rigorous gross lift	1086	g
Engineering 1 g/l lift (design figure)	953	g
Helium lift at the same conditions (for reference)	1006	g
Hydrogen-over-helium advantage	+8.0	%

6. Envelope Material Selection

Five criteria drove the material selection. The envelope must have low gas permeability, particularly for hydrogen, which is a smaller molecule than helium and diffuses correspondingly faster through many polymers. It needs UV and weather resistance for outdoor use. It needs to be heat-sealable, since adhesive bonding adds mass and weak points. It needs to be usable at the lower temperatures.

Dhawan and Jindal’s review of polyurethane in LTA systems [19] is the cleanest single reference for the trade. Polyurethane (PUR) is the strongest all-round flexible-polymer candidate: low gas permeability, good UV resistance, excellent bendability and excellent low-temperature behaviour. Chatterjee et al. [20] showed that adding a few percent of montmorillonite nanoclay or graphene to PUR and cut gas transmission further still by

lengthening the diffusion path that a permeating molecule has to transverse. Adak and Joshi's [21] chapter on coated and laminated aerostats textiles in the border reference for multilayer hull constructions, including the BoPET (biaxially oriented polyethylene terephthalate) and PVF (Tedlar®) options that improve UV performance at the cost of bendability. PET specifically has been validated on small drones such as the S-CLOUD platform of Song et al. [12,13] who used 35-micron PET sealed at about 210° C and held it for over an hour in flight.

For the hydrogen-specific permeability question, Checchetto [22] measured light-gas transport (H_2, He, N_2, CO_2) through LDPE between 295 K and 350 K and reported permeability coefficients that are within roughly a factor of two of those for helium which are close enough that the engineering implications for a 90 minute sortie are negligible. Lee et al. [23] compared volumetric permeation of H_2, He, N_2, O_2 and Ar through polyethylene at elevated pressure and confirmed the same broad ranking. Ultra-thin biaxially-oriented PET (BoPET) and aluminized mylar films represent further lightweight options within the same family, as suggested by Adak et al. [24]. Table 4 summarises the comparison drawn from these sources.

Table 4 Candidate envelope material comparison (synthesized from [19], [22], [21], [23])

Material	H_2 barrier	UV/weather	Bonding	Flex fatigue	Heat seal	Mech. Properties	Low temp
PUR	Low	Good	Excellent	Good	Yes	Fair- Good	Excellent
PET	Low	Fair	Fair	Fair	No	Fair	Fair
PVF	Low	Excellent	Poor	Excellent	No	Fair	Poor
PVC	Fair	Good	Excellent	Good	Yes	Excellent	Poor
LDPE	Fair	Fair	Poor	Excellent	Yes	Fair	Good

For the prototype, LDPE was chosen on the grounds of cost, availability and fabrication ease. It seals reliably at 110-130° C using an impulse sealer, comes in commercial widths up to 6 m, offers serviceable hydrogen-barrier over a single sortie. For the production platform we intend to move to a PUR- based multilayer envelope along the lines of [20,21], which will improve both gas-retention and UV-resistance at the most of higher unit price.

7. Mass Architecture

7.1 Component mass budget

Table 5 gives the full mass breakdown of the prototype. The propulsion choice is three T-motor F60 Pro IV 2306.5 brushless motors at 1950 KV, driven by an F45A 4-in-1 ESC and a F7 flight controller with MPU6000 IMU which is deliberately overspecified for the residual thrust requirement: the same hardware will support the wind-disturbance margin once outdoor operations begins. The 1300 mAh 4S LiPo battery and 80 g of trim ballast complete the airframe-side mass, and the 500 g payload allocation is sized for a representative multispectral camera and IMU/GPS package.

Table 5 Component mass breakdown of the buoyant UAV

Component	Specification	Qty	Total Weight (g)
Payload	Cameras, sensors, mount	1	500
Brushless motors	T-Motor F60 Pro IV 2306.5, 1950 KV	3	92.4
Flight controller	F7, MPU6000 IMU	1	5.1
ESC (4-in-1)	F45A 4-in-1	1	9.2
Battery	1300 mAh, 4S LiPo (14.8 V), 120 C	1	150
Envelope	LDPE thin-film, heat-sealed	1	190
Carbon-fibre frame	Concentric inner + outer ring	1	78.8
Trim ballast	Adjustable	1	80
All-up mass, W	-	-	1105.5

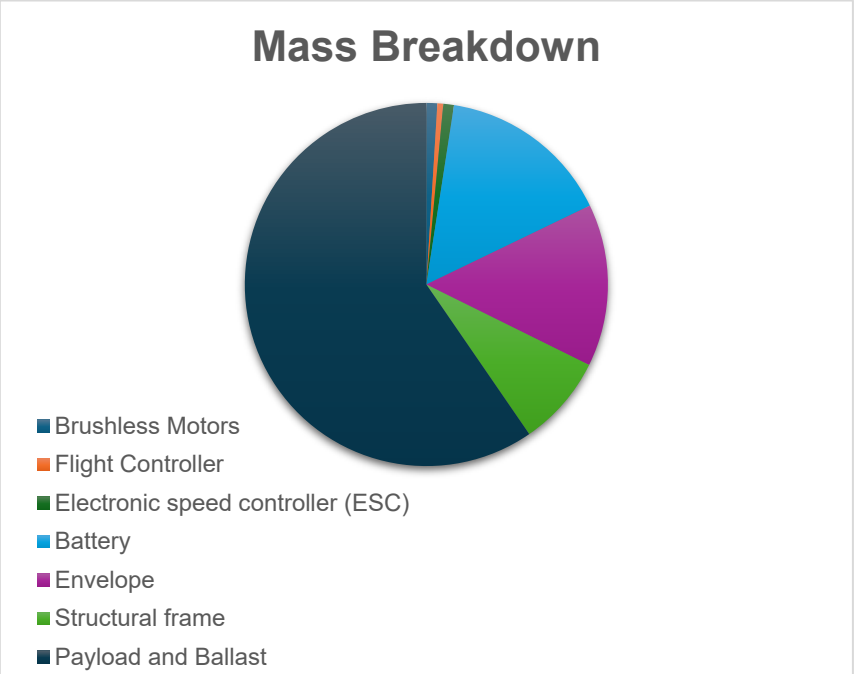


Figure 3 Mass breakdown of the buoyant UAV by component group

Payload and ballast account for 52.5 % of the 1105.5 g all-up mass: battery and envelope add another 17.2 % and 13.6 % respectively: the carbon fiber ring is 7.1 % and the entire propulsion stack (three motors plus the 4-in-1 ESC) sits under 9.2 % and the flight controller at under 1 %. For comparison, the scaling laws fitted by Ardelean et al. [25] across small unmanned wingless rotorcraft put the typical payload mass fraction at 15-30 % of all-up. The present platform is well above the range because hydrogen buoyancy is doing the work that a multirotor's structure and propulsion would have to do.

7.2 Buoyancy & thrust balance

With the conservative engineering lift ligure of 953 g against the 1105.5 g all up mass, hydrogen buoyancy covers 86.2% of the system weight. The propulsion system needs to supply only the residual 153 g of vertical thrust at hover which is distributed across three motors, that is roughly 51 g per motor, far below the rated output of F60 pro IV. Using the ISA-rigorous lift figure of 1086 g instead, the residual drops to only 19 g (about 6 g per motor), reflecting how closely the platform sits to neutral buoyancy under best-case gas-purity and temperature conditions. The realised hover throttle in the field will sit between these two figures, with the precise value depending on ambient temperature, residual envelope air and inflation pressure. Either way, hover sits at a very low throttle setting, and the corresponding battery current draw is what gives the platform its endurance advantage over a conventional multirotor. Table 6 collects the buoyancy and thrust figures.

Table 6 Buoyancy and thrust balance

Parameter	Value	Units
Envelope volume	0.9529	m^3
Design gross H_2 lift	953	g
ISA rigorous gross H_2 lift	1086	g
All-up mass, W	1105.5	g
Buoyancy ratio (ISA-rigorous)	98.2	%
Residual hover thrust	≈ 19 - 153	g
Thrust per motor	≈ 6 - 51	g

7.3 Structural concept

The structure is two concentric carbon-fibre tubular rings. The outer ring runs around the envelope's maximum diameter circumference and gives the envelope its peripheral shape: it also carries the two outboard brushless motors and the ESC. The inner ring sits inside the central bore ($Dgap = 0.154\,m$) and carries the vertical lift motor, the flight controller and the battery, holding the centre of mass on the axis of revolution. Carbon-fibre tube was chosen on strength-to-weight grounds. The combined inner + outer ring mass is 78.8 g, which is 7.1 % of all up mass which is well below structural fraction of a comparable multirotor at the same payload and broadly consistent with the structural scaling reported for OSIRCA [9] and for small rotorcraft generally [25]. Full structural finite-element analysis under combined buoyancy, payload and wind-gust loading is under way and will be reported separately.

7.4 Wiring and electrical layout

Figure 4 shows the electrical layout of the prototype. The 1300 mAh 4S LiPo battery supplies 14.8 V power directly into flight controller and the 4-in-1 ESC, which together form the two power distribution nodes of the system. The ESC drives the three brushless motors over three phase output, one phase set per motor, with each motor receiving an independent throttle control. The flight controller, send the throttle commands to the ESC and controls the two vectoring servos, each mounted under the motors directly. Tilting the outboard motors with these servos rather than relying on differential thrust alone gives the platform finer pitch and yaw authority at low residual thrust. All signal and power leads are planned to be routed along the inner carbon-fibre ring and held by short cable ties at each motor and servo mounts to prevent any contact with the envelope wall.

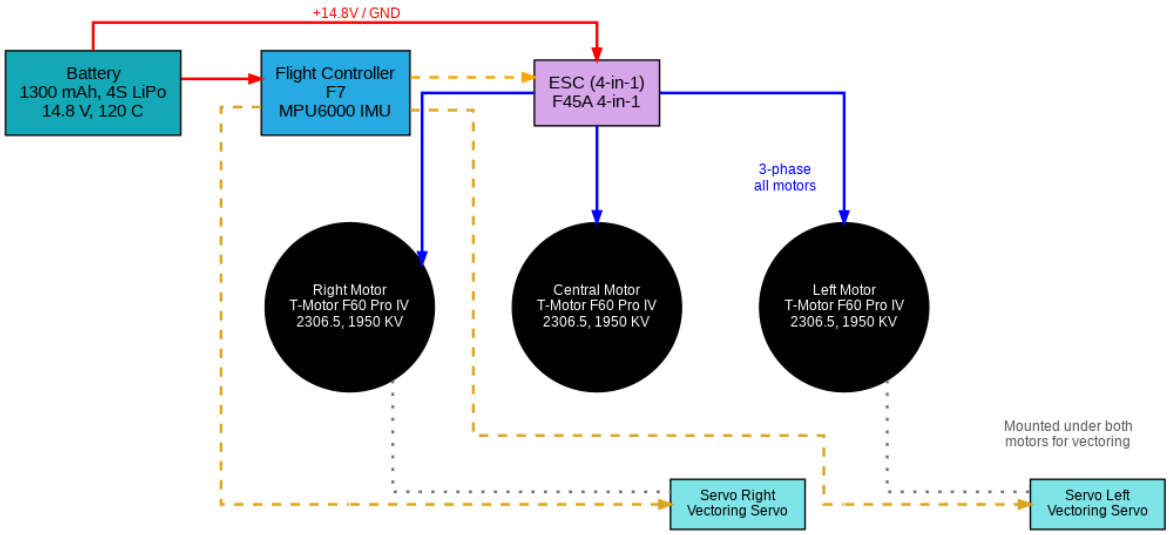


Figure 4 Electrical layout of the buoyant UAV

8. Hydrogen Safety Considerations

Choosing hydrogen over helium imposes a real engineering responsibility, and it is worth saying clearly what the hazards are and what they are not. The Hindenburg image looms large in public imagination, but the dominant failure mode for a sealed hydrogen envelope is not in-flight combustion, it requires both an ignition source and an oxidiser inside the envelope, neither of which is present during normal operation. The real risks are concentrated at three points in the operational cycle: ground handling and inflation, gradual permeation and accumulation in enclosed spaces, and rapid venting following an envelope rupture. Each of these has a well-established mitigation, and the modern airship and scientific-balloon community has codified them as seen in Khoury and Gillett's reference text [18] for the airship-engineering treatment and NASA's 2025 return-to-hydrogen briefing for the scientific-ballooning position [5].

For the present platforms, the operational measures we have adopted are:

- Inflation is carried out outdoors only, on open grounds, with no overhead structure and a clearly demarcated 5 m seclusion zone enforced during gas transfer.

- Industrial- grade hydrogen (≥ 99.9 % purity) is used to minimize combustible mixture formation during routine inflation: the regulator is fitted with a one-way check valve to prevent back-flow.
- The envelope is heat-sealed in single passes and pressure-tested before inflation: pinhole leaks are identified by soap-water swabbing. A static-vent step before each sortie displaces any residual air left over from manufacturing.
- All operations are conducted indoors in a large, well-ventilated space with mechanical air change adequate to keep any localised hydrogen concentration well below the lower flammability limit, never in small or unventilated rooms.

With these measures in place, the operational risk profile is no more onerous than the standard practice for hydrogen filled meteorological balloons, which are released routinely by national weather services across the world. The cost and availability arguments documented in [5], specifically that hydrogen is five to ten times cheaper than helium and is available worldwide, make the hydrogen choice both economically and logistically defensible. Bock and Künkler reached the same conclusion for a much larger lenticular platform a decade earlier [4].

9. Prototype Build and Initial Flight

9.1 Sub-scale validation prototype

Before committing to the full-scale build, we built a sub-scale prototype to shake out the control and integration questions cheaply. Rather than designing one from scratch, we started from a commercially available toy blimp, which gave us a ready-made thin film envelope and a small electronics package (motors, receiver and battery holder) at very low cost. The toy as supplied was structurally broken on arrival and it was not possible to buy another as it was very old and very hard to find due to its age and would have not flown in its original form, so the entire airframe was rebuilt. The original frame was discarded, a new 3D-printed PLA frame was designed, and the motor orientation was changed from the toy's layout to the configuration that matches the full-scale platform. The salvaged envelope is the primary gas cell, and a small secondary balloon mounted on top is used as a tuneable trim volume whose inflation level dials the buoyancy margin exactly against the as-built airframe. Control is by the original hobby RC receiver, powered by CR123A cell, with one motor handling vertical motion and the other two handling pitch and yaw. Structural mass excluding the envelope is about 63 g: envelope plus trim balloon adds a further 10 g, bringing the total to 73 g. The sub-scale prototype confirmed that a buoyant platform can hover and manoeuvre with minimal onboard mass, and it gave us the control mapping we needed for the full-scale build.



Figure 5 Sub-scale validation prototype

9.2 Full-scale prototype

The full-scale prototype was assembled to the principal dimensions of Table 2. At the time of the first flight the outer carbon-fibre ring was not yet available, so the prototype was flown with the inner ring and lift motors only: the two outboard motors were temporarily attached to the envelope via fabric tabs. The build confirmed envelope to frame fit, motor and ESC routing, and the placement of the battery and flight controller on the inner ring.



Figure 6 Initial Prototype



Figure 7 Initial Flight

9.3 Initial flight observations

Initial indoor flight confirmed that first-principals design assumptions. The platform achieved and held controlled hover, with manoeuvre authority adequate for slow transitional motion. Lift was achieved by the central motor; pitch authority was noticeably softer than designed because the outer ring was absent: installing it is expected to recover the designed pitch stiffness. Yaw authority was adequate for the planned slow-cruise mission profile. Quantitative endurance, current-draw and outdoor-wind characterisation are scheduled for the next test campaign.

10. Conclusion and Future Work

We have presented the design and first prototype of a hydrogen-filled toroidal lenticular buoyant UAV for near canopy precision-agricultural surveillance. The main outcomes are the following: a closed-from analytical formula has been derived for the envelope volume of the chosen geometry and verified against CAD measurement to four decimal places at Φ = 4.0, $Vtotal = 0.9529\, m^3$. With hydrogen as the lifting gas, the envelope delivers 1086 g of theoretical lift at ISA conditions and 953 g under the conservative engineering rule used for sizing, against an all up mass of 1105.5 g which means the buoyancy ratio sits between 86 % and 98 % depending on which lift figure is used, with the propulsion system left to supply between 6 and 51 g of thrust per motor at hover. The 52.5 % payload and ballast fraction is well above the 15 - 30 % typical of small multirotors. A working sub-scale and full-scale prototype have demonstrated initial controlled hover.

The next milestone is straightforward and already under way. The outer carbon ring needs to be fitted to recover the designed shape, the autopilot needs to be tuned for outdoor station keeping, the drag coefficient at Φ = 4.0 needs to be validated by CFD against the precedent data of Kanoria et al. [6]; and the payload needs to be integrated and characterised in flight. Once consistent indoor hover is demonstrated end-to-end, we move to outdoor field trials over real crop canopies, where the wind-disturbance behaviour, the solar-warming response of the envelope and the full-day endurance figure will be measured directly.

11. Contact Author Email Address

Corresponding author: Pruthvi P. Kapoor, mailto: pruthvikapoor59@gmail.com

12. Copyright Statement

The authors confirm that they, and/or their company or organization, hold copyright on all of the original material included in this paper. The authors also confirm that they have obtained permission, from the copyright holder of any third party material included in this paper, to publish it as part of their paper. The authors confirm that they give permission, or have obtained permission from the copyright holder of this paper, for the publication and distribution of this paper as part of the ICAS proceedings or as individual off-prints from the proceedings.

References

[1] Zhang, H., Wang, L., Tian, T., and Yin, J., "A Review of Unmanned Aerial Vehicle Low-Altitude Remote Sensing (UAV-LARS) Use in Agricultural Monitoring in China," Remote Sensing, Vol. 13, No. 6, 2021, p. 1221. https://doi.org/10.3390/rs13061221

[2] Macias, G. and Lee, K., "Design and Analysis of a Helium-Assisted Hybrid Drone for Flight Time Enhancement," American Journal of Engineering and Applied Sciences, Vol. 15, No. 4, 2022, pp. 316–330. https://doi.org/10.3844/ajeassp.2022.316.330

[3] Yang, Shenghui & Xu, Pingfan & Jiang, Shijie & Zheng, Yongjun. (2022). Downwash characteristics and analysis from a six-rotor unmanned aerial vehicle configured for plant protection. Pest Management Science. 78. 10.1002/ps.6790. https://doi.org/10.1002/ps.6790

[4] Bock, J.K. and Künkler, H., "Concept of a Lenticular Hybrid Airship Using Hydrogen for Multiple Operation Modes," 10th International Airship Convention (SLTA), Ganderkesee, 2015. dglr.de/publikationen/2015/380021.pdf

[5] Roth S and Reed E. Hydrogen ballooning. *Scientific Ballooning Technologies Workshop*, NASA Goddard Wallops Flight Facility Balloon Program Office, St. Paul MN, 14-16 May 2025. NASA NTRS 20250004774. https://ntrs.nasa.gov/citations/20250004774

[6] Kanoria, A.A., Pant, R.S., and Shah, T.K., "Conceptual Sizing and Design of a Lenticular Aerostat," 9th International Airship Convention, Ashford, 2012. https://www.researchgate.net/publication/257307540_Conceptual_Sizing_and_Design_of_Lenticular_Aerostat

[7] Lobner, P., "C.N.R.S. Pégase — Lenticular Stratospheric Airship," Modern Airships Series, February 2022. https://lynceans.org/wp-content/uploads/2021/08/CNRS_Pegase-converted.pdf

[8] Lobner, P., "DKBA (ДКБА) — Lenticular Airships," *Modern Airships, Part 1*, Lyncean Group of San Diego, 11 February 2022. https://lynceans.org/wp-content/uploads/2022/02/DKBA-lenticular-airships-converted.pdf

[9] Gnanaprakash, K., Kamalraj, K.P., and Pant, R.S., "Design-Build-Fly of OSIRCA: Oblate Spheroid Indoor Remotely Controlled Airship," 11th AIAA ATIO Conference, Virginia Beach, 2011. https://doi.org/10.2514/6.2011-6914

[10] Bock, J. K., Apel, U., and Van Treuren, R. G., "Lenticular Cargo Airships: The Case for Carbon-Free Fuel Operation," AIAA Aviation 2019 Forum, Dallas. https://doi.org/10.2514/6.2019-2862

[11] Manikandan M and Pant R S. Research and advancements in hybrid airships — A review. *Progress in Aerospace Sciences*, Vol. 127, 100741, 2021. https://doi.org/10.1016/j.paerosci.2021.100741

[12] Song, S.H., Shon, H.W., Yeon, G.Y., and Choi, H.R., "Design and Implementation of Cloud-Like Soft Drone S-CLOUD," 2018 IEEE/RSJ IROS, Madrid. https://doi.org/10.1109/IROS.2018.8593601

[13] Song, S.H., Yeon, G.Y., Shon, H.W., and Choi, H.R., "Design and Control of Soft Unmanned Aerial Vehicle 'S-CLOUD'," IEEE/ASME Transactions on Mechatronics, Vol. 26, No. 1, 2021, pp. 267–275. https://doi.org/10.1109/TMECH.2020.3013256

[14] Song, S.H. and Choi, H.R., "Design, Control and Implementation of Torus-Type Omni-Orientational Blimp with Tilting Actuators," IEEE Access, Vol. 9, 2021, pp. 147985–147993. https://doi.org/10.1109/ACCESS.2021.3123355

[15] Cho S, Mishra V, Tao Q, Varnell P, King-Smith M, Muni A, Smallwood W and Zhang F. Autopilot design for a class of miniature autonomous blimps. *Proc. 2017 IEEE Conf. on Control Technology and Applications (CCTA)*, Kohala Coast, pp 841-846, 2017. https://doi.org/10.1109/CCTA.2017.8062564

[16] Seguin, L., Zheng, J., Li, A., Tao, Q., and Zhang, F., "A Deep Learning Approach to Localization for Navigation on a Miniature Autonomous Blimp," 2020 IEEE 16th ICCA, Sapporo, pp. 1130–1136. https://doi.org/10.1109/ICCA51439.2020.9264514

[17] Yamada, W., Manabe, H., and Ikeda, D., "Blade-Free Drone," NTT DOCOMO Technical Journal, Vol. 21, No. 4, 2020, pp. 37–43. [ZeRONE: CHI 2019. https://doi.org/10.1145/3290605.3300595]

[18] Khoury, G.A. and Gillett, J.D. (eds.) (1999) *Airship technology*. Cambridge: Cambridge University Press. Available at: https://archive.org/details/airshiptechnolog0000unse

[19] Dhawan, A. and Jindal, P., "A Review on Use of Polyurethane in Lighter-than-Air Systems," Materials Today: Proceedings, Vol. 43, 2021, pp. 746–752. https://doi.org/10.1016/j.matpr.2020.12.962

[20] Chatterjee, U., Butola, B. S. and Joshi, M. (2016), Optimal designing of polyurethane-based nanocomposite system for aerostat envelope. J. Appl. Polym. Sci., 133, 43529. https://doi.org/10.1002/app.43529

[21] Lv J, Zhou Y, Zhang Y, Nie Y and Wang Q (2022) Study of performance of aerostat envelope materials on the coast. Front. Mater. 9:992984. doi: 10.3389/fmats.2022.992984

[22] Checchetto, Riccardo, Experimental Study on the Transport of Light Gas Molecules through Low-Density Polyethylene Films, International Journal of Polymer Science, 2018, 4903904, 9 pages, 2018. https://doi.org/10.1155/2018/4903904

[23] Lee, J.-H., Kim, Y.-W., & Jung, J.-K. (2023). Investigation of the Gas Permeation Properties Using the Volumetric Analysis Technique for Polyethylene Materials Enriched with Pure Gases under High Pressure: H_2, He, N_2, O_2 and Ar. *Polymers*, *15*(19), 4019. https://doi.org/10.3390/polym15194019

[24] Adak, B. and Joshi, M. (2018). Coated or Laminated Textiles for Aerostat and Stratospheric Airship. In Advanced Textile Engineering Materials (eds S. ul-Islam and B.S. Butola). https://doi.org/10.1002/9781119488101.ch7

[25] Ardelean, I.C., Usov, D., Filippone, A., Parslew, B., and Hollingsworth, P., "Unmanned Wingless Rotorcraft Scaling," *Journal of Aircraft*, Vol. 60, No. 5, 2023, pp. 1553–1563. https://doi.org/10.2514/1.C037299